Strategies reimagined: SDG-driven solutions for combating global desertification

Xunming Wang[a,b] (ID), Xin Geng[a,b,1] (ID), Fubao Sun[a,b,1], Mengyao Han[a], Fahu Chen[b,c], Shengqian Chen[c], Josep Peñuelas[d] (ID), Lei Gao[e], Brett A. Bryan[f] (ID), Changjia Li[g,h] (ID), Lindsay C. Stringer[i,j] (ID), Jiansheng Ye[k] (ID), Siyu Chen[l], Jimin Sun[m], Huayu Lu[n] (ID), Huizheng Che[o], Hongyan Liu[p] (ID), Baoli Liu[q,r] (ID), Zhibao Dong[s], Shixiong Cao[t], Ting Hua[u], Xin Gao[v], Zhenting Wang[w] (ID), Zhaosheng Wang[a] (ID), Diwen Cai[a] (ID), Duanyang Xu[a], Wenbin Zhu[a] (ID), Zhiyang Lan[a], Wenbin Liu[a] (ID), Hong Cheng[g], Shi Hu[a] (ID), Mingxing Chen[a] (ID), Jie Li[a] (ID), Danfeng Li[a], Fa Liu[a], Shuying Zhang[a], Yuan Gong[a] (ID), and Zhepeng Dong[a]

Affiliations are included on p. 9.

Desertification threatens 24% of the world's land area across 126 countries and affects 35% of the global population. However, mainstream global efforts to combat desertification prioritize short-term vegetation greening over addressing resource constraints and local livelihoods, posing hidden challenges to long-term Sustainable Development Goals (SDGs) attainment. Here, we evaluated the socioeconomic trade-offs of China's long-standing desertification reversal strategies and explored the potential benefits of innovative agricultural practices using high-resolution suitability models for major crops and cultivated pasture. Compared with a no-intervention baseline, continuing the Grain-for-Green Program and grazing exclusion under projected 2023–2050 warming and wetting trends would lead to reductions of up to 54 to 55% in grain output, 81% in livestock production, and 61% in agricultural income. Conversely, strategies emphasizing pasture cultivation and crop switching could substantially lower national expenditures on combating desertification while restoring ecosystems, enhancing agricultural productivity and incomes, and conserving water resources. These benefits would contribute 0.7%, 9.8%, and 3.8% toward global progress on SDG 1 (no poverty), SDG 2 (zero hunger), and SDG 6 (clean water and sanitation), respectively, while exhibiting trade-offs across multiple SDGs. This study provides a reimagined strategy framework for combating global desertification and promoting sustainable development in vulnerable arid regions worldwide.

desertification | sustainable development goal | policy rectification | climate-economic system

Desertification—land degradation in arid, semiarid, and dry subhumid areas resulting from climatic variability and human activities (1)—affects 24% of the global land surface across 126 countries, threatening ecosystem stability and the livelihoods of 35% of the world's population (1–3). Current global efforts to combat desertification, typically involving reforestation, grazing exclusion, and cropland retirement, aim to reverse land degradation, enhance carbon sequestration, and improve climate resilience (4–6). However, these strategies prioritize short-term vegetation greening over resource constraints and local livelihoods, limiting progress toward the Sustainable Development Goals (SDGs) (7). China represents a critical case in combating global desertification, with 44% of its territory falling within desertification-prone regions, climatically defined as areas with an aridity index <0.5 that are highly vulnerable to land degradation, independent of vegetation cover or soil type (1, 8; *SI Appendix,* Fig. S1). Since 1978, China has launched extensive desertification reversal strategies (*SI Appendix,* Fig. S2), achieving partial success at the national scale (9–11). These strategies have been integrated into the policy framework of the 197 parties to the United Nations Convention to Combat Desertification (UNCCD) and directly adopted by more than 50 countries (3, 9). Yet despite 1.30 trillion RMB (~185 billion USD) invested between 2000 and 2020 (*SI Appendix,* Figs. S2 and S3) and the resulting reduction in agricultural productivity, desertification persists, causing annual economic losses of 33.3 to 96.9 billion RMB (4.7 to 13.8 billion USD) (12). Substantive and integrative solutions to these conflicts remain urgently needed.

Coordinating multiple SDGs related to desertification and livelihoods is inherently challenging. Extreme poverty and water scarcity (3, 13, 14), combined with agriculture's substantial share of GDP in desertification-prone regions and its crucial role in global food security (15), create unavoidable regional disparities. Conventional interventions, such as large-scale afforestation and restrictive land management, that were widely implemented in China, the Sahel, and Saudi Arabia, generally exacerbate tensions among ecological

Significance

Desertification threatens nearly a quarter of global land across 126 countries, affecting over one-third of the population. Current efforts to combat desertification mainly prioritize short-term greening while overlooking water security and local livelihoods. We quantify measures to combat desertification and demonstrate the potential of innovative agricultural practices that balance socioeconomic development with ecological restoration. Compared with conventional strategies, our proposed strategies emphasizing pasture cultivation and crop switching—could lower national costs of combating desertification while simultaneously restoring ecosystems, boosting agricultural productivity, improving rural incomes, and strengthening water security under projected warming and wetting trends over the next three decades. Using China as a representative case, these reimaged strategies offer a comprehensive yet practical pathway toward achieving the Sustainable Development Goals.

restoration (16, 17), social stability (18), and economic viability (4). While agriculture has historically been a major driver of land degradation (2, 19), evidence from numerous desertification-prone countries across the Middle East and North Africa (20–22) demonstrated that advances in pasture cultivation and crop switching can simultaneously increase productivity, reduce water use, and maintain vegetation cover. Embedding such practices into desertification reversal strategies and rigorously evaluating their multidimensional SDG cobenefits offers a transformative pathway to reconcile environmental and socioeconomic goals (23). Given its extensive desertification-prone regions and history of large-scale interventions, China provides a critical testbed for these innovations.

Here, we assess the trade-offs between China's conventional desertification reversal strategies since 1999 including the Grain-for-Green Program, which compensates farmers for converting unsuitable cropland into forest or grassland to promote ecological restoration as well as soil and water conservation, and grazing exclusion via fencing to restore natural vegetation (*Materials and Methods*). Using high-resolution local data and statistical learning models, we developed suitability and yield assessment models for major crops, natural grasslands, and cultivated pastures. These models were applied to compare agricultural productivity and income trends over the past 60 y (1961–2022) under two scenarios: 1) full implementation of the Grain-for-Green Program with grazing exclusion, and 2) a baseline without interventions, to evaluate the socioeconomic sustainability of current strategies. We further examine how optimized agricultural practices, including pasture cultivation and crop switching, can combat desertification while generating coordinated socioeconomic and ecological cobenefits. Using climate projections from the Coupled Model Intercomparison Project Phase 6 (CMIP6) as inputs, we project trends in agricultural suitability, production, and income from 2023 to 2050 under future climate scenarios. Building on these projections, we design specific practical strategies and evaluate their socioecological outcomes. Finally, we discuss pathways for integrating SDGs into policy frameworks and propose reimagined strategies to combat global desertification.

Results

Trade-Offs between Combating Desertification and Enhancing Agricultural Sustainability.

Using multiyear averages of climatic, topographic, soil, land use, and socioeconomic conditions, we evaluated both the scale and intensity of China's desertification reversal strategies and their alignment with regional ecological carrying capacity and agricultural sustainability before (1961–1999) and after (2000–2022) the implementation of the Grain-for-Green Program and grazing exclusion (*Materials and Methods*). Our results indicated that 30.7% of cultivated cropland in desertification-prone regions was unsuitable for farming between 1961 and 1999 (Fig. 1 *A* and *E* and *SI Appendix*, Fig. S4). Despite extensive efforts since 2000 (*SI Appendix*, Fig. S2), only 2.0% of marginal cropland was effectively rehabilitated, while 23.9% of cultivated cropland remained unsuitable during 2000–2022 (Fig. 1 *C* and *E* and *SI Appendix*, Figs. S5 and S6). From 1961 to 1999, these regions supported an annual average of 1.74 billion sheep units (SUs), with 47.9% grazing on natural grasslands and 52.1% barn-fed; notably, 18.4% of SUs relied on forage grown on unsuitable cropland (Fig. 1 *B* and *E*). Between 2000 and 2022, livestock capacity increased by 6.2%, with 51.7% grazing on natural grasslands and 48.3% barn-fed, while 12.6% still depended on unsuitable cropland (Fig. 1 *D* and *E*). These patterns reveal limited relief of pressure on ecologically unsuitable lands and suboptimal strategies implementation.

Vegetation restoration remains the primary goal of existing conventional strategies, however, these measures inadvertently constrain farming and rural livelihoods without attention to agricultural viability. Using current agricultural practices as the baseline, we further simulated a full-implementation scenario under 2000–2022 climatic conditions in which all unsuitable cropland and natural grasslands were retired. Compared with the no-intervention scenario, full implementation of the Grain-for-Green Program and grazing exclusions would reduce annual grain output by 26.0%, livestock production by 64.2%, and cash crop output by 14.6%, while cutting annual household incomes for farmers and herders in desertification-prone regions by 46.2% (Fig. 1 *F* and *G*). Nationally, grain and livestock production would decline by 4.1% and 11.5%, respectively, resulting in a 0.2% decrease in gross domestic product (GDP) by 0.2%.

Impacts of Future Climate Change on Combating Desertification.

The impacts of climate change on conventional strategies for combating desertification remain uncertain, while existing implementation strategies may have already led to suboptimal development in relevant regions. To address this, we applied a Bayesian ensemble average of multiple CMIP6 models to generate daily climate projections under three future scenarios combining Shared Socioeconomic Pathways (SSPs) and Representative Concentration Pathways (RCPs). These scenarios represent key future baselines: L1 (SSP1-2.6, low warming with sustainable development and aggressive emission reductions), M2 (SSP2-4.5, moderate warming with intermediate development and mitigation), and H3 (SSP5-8.5, high warming with fossil-fueled growth and minimal mitigation) (*SI Appendix, Supporting Text*). Changes in annual agricultural production and income in China's desertification-prone regions from 2023 to 2050 were then recalculated by rerunning suitability and yield assessment models with projected climate inputs, while holding soils and terrain constant. This approach enabled the assessment of potential implications of maintaining current desertification reversal strategies through 2050.

We found that future climate change is projected to reduce farmland productivity while enhancing pastoral carrying capacity, suggesting that maintaining current desertification reversal strategies could exacerbate agricultural losses (Fig. 2). Compared to 2000–2022 averages, grain output in desertification-prone regions is projected to decrease by 5.3 ± 1.5% under L1 and by 5.8% under both M2 (±1.6%) and H3 (±1.4%) (Fig. 2*C*) during 2023–2050. Conversely, livestock production is projected to increase by 5.9 ± 4.8% under L1, 9.2 ± 4.8% under M2, and 12.0 ± 7.9% under H3 (Fig. 2*D*). These projections suggest future climate change will negatively impact grain production but may create opportunities for livestock expansion, especially under moderate (M2) and high (H3) warming scenarios. However, continuing the Grain-for-Green Program and grazing exclusion is projected to cause sharp declines, including crop output losses of 54.0% (M2) to 55.2% (L1), livestock production losses of 80.7% (L1) to 81.4% (H3), and income losses for farmers and herders of 60.9% (M2) to 61.7% (H3) relative to the no-strategy baseline (Fig. 2 *C–E*).

In addition, the potential opportunities presented by climate change should not be overlooked, particularly increased soil moisture and expanded suitable cropping areas. Here, we projected significant increases in root-zone soil moisture—derived from multiple reanalysis products—across all climate scenarios (L1, M2, and H3) from 2023 to 2050 in China's desertification-prone regions (*SI Appendix*, Fig. S7 and *Supporting Text*), which substantially shifts optimal agricultural practices. Suitability assessments indicated that crop-suitable area expanded by 9.8% (L1), 12.3%
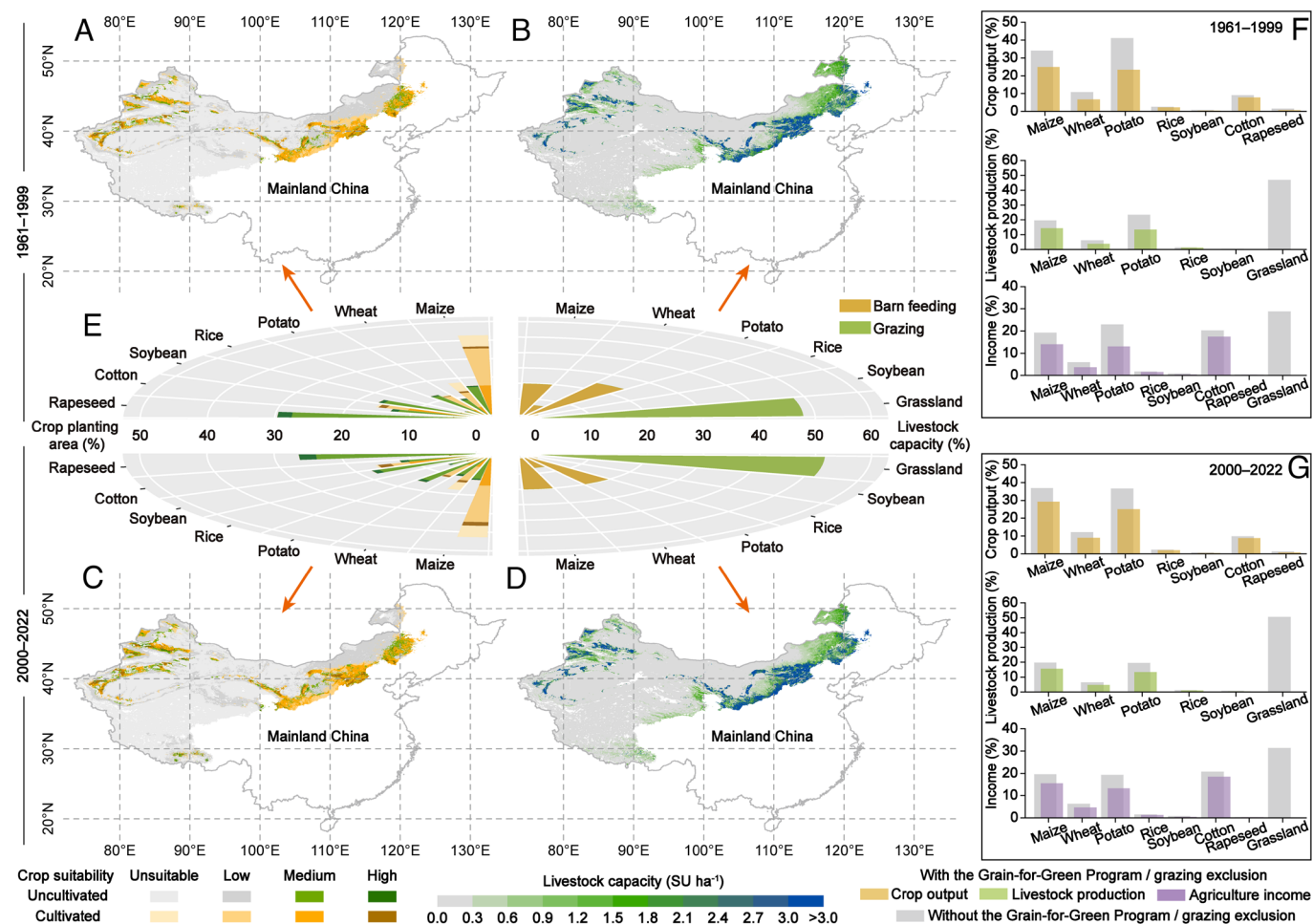
Fig. 1. Crop suitability, livestock capacity, agricultural production, and agricultural income in China's desertification-prone regions before (1961–1999) and after (2000–2022) the implementation of the Grain-for-Green Program and grazing exclusion. Panels (*A*) and (*B*) display the spatial distributions of crop suitability and livestock capacity for 1961–1999, respectively. Panels (*C*) and (*D*) display the corresponding distributions for 2000–2022. Livestock capacity reflects the carrying capacity of natural grasslands combined with barn feeding supported by feed crops (maize, wheat, rice, soybeans, and potatoes). The *Top-Left* and *Bottom-Left* charts in panel (*E*) show crop suitability statistics for maize, wheat, potatoes, rice, soybeans, cotton, and rapeseed across four levels (unsuitable, low, medium, high), derived from Panels (*A*) and (*C*). These charts also display the proportion of nonarable land classified as moderately or highly suitable within total available land, excluding undeveloped areas deemed unsuitable or of low suitability for antidesertification efforts. The *Top-Right* and *Bottom-Right* charts in panel (*E*) show the proportion of livestock capacity attributed to feeding crops and grasslands relative to the total regional livestock population in Panels (*B*) and (*D*). Panels (*F*) and (*G*) present regional agricultural production statistics and related incomes for 1961–1999 and 2000–2022, respectively. Gray bars represent the production and incomes under current agricultural practices, while colored bars—yellow for crop output, green for livestock production, and purple for agricultural income—denote the outcomes after retiring unsuitable/low-suitability cropland and excluding grazing on natural grasslands. All data are expressed as percentages of the actual regional total production and income. Actual areas abandoned and impacts observed during desertification combating in 2000–2022 are shown in *SI Appendix*, Fig. S5. Independent crop suitability assessments for both periods are shown in *SI Appendix*, Figs. S4 and S6.

(M2), and 11.3% (H3) under 2023–2050 climatic conditions compared with 2000–2022 levels (Fig. 2*A* and *SI Appendix*, Fig. S8), with more than 70% of the expansion occurring on currently uncultivated cropland. Simultaneous, natural grasslands' carrying capacity is projected to increase by 16.3 ± 7.9% under L1, 23.3 ± 7.8%, under M2 and 28.6 ± 14.0% under H3 (Fig. 2*B*). Trade-offs make it possible to consider optimizing agricultural and pastoral land use patterns as an alternative to current desertification reversal strategies. Building on this foundation, proactively adjusting agricultural practices, including expanding cultivation in newly suitable areas and adopting innovative farming systems, could therefore enhance economic resilience while combating desertification under future climate scenarios.

Reimagined Strategies to Combat Desertification under Future Climate Scenarios. To address the opportunities arising from climate change, we evaluated six advanced agricultural practices (Table 1 and *SI Appendix*, Fig. S9) for their impacts on vegetation

cover, crop output, livestock production, agricultural income, and ecological water deficits in China's desertification-prone regions from 2023 to 2050 under scenarios L1, M2, and H3 (Fig. 3 and *SI Appendix*, Figs. S10–S14). These indicators were selected in consideration of their ability to capture the sustainability of desertification reversal strategies and their direct relevance to SDG priorities such as hunger alleviation, poverty reduction, and water sustainability (*SI Appendix*, Table S1). The baseline scenario (S0) reflects current agricultural practices without additional interventions, serving as the reference for assessing strategy outcomes. Given high interannual variability, average climatic conditions for 2023–2050 were used as model inputs to evaluate each scenario and proposed strategies.

Our findings revealed that the conservative land-retirement strategy (S1) could effectively reduce regional ecological water deficits by 20.7 to 22.3%. However, it also decreases crop output by 21.3 to 22.9%, livestock production by 6.6 to 7.6%, agricultural income by 10.0 to 11.0%, and vegetation cover by 0.8 to
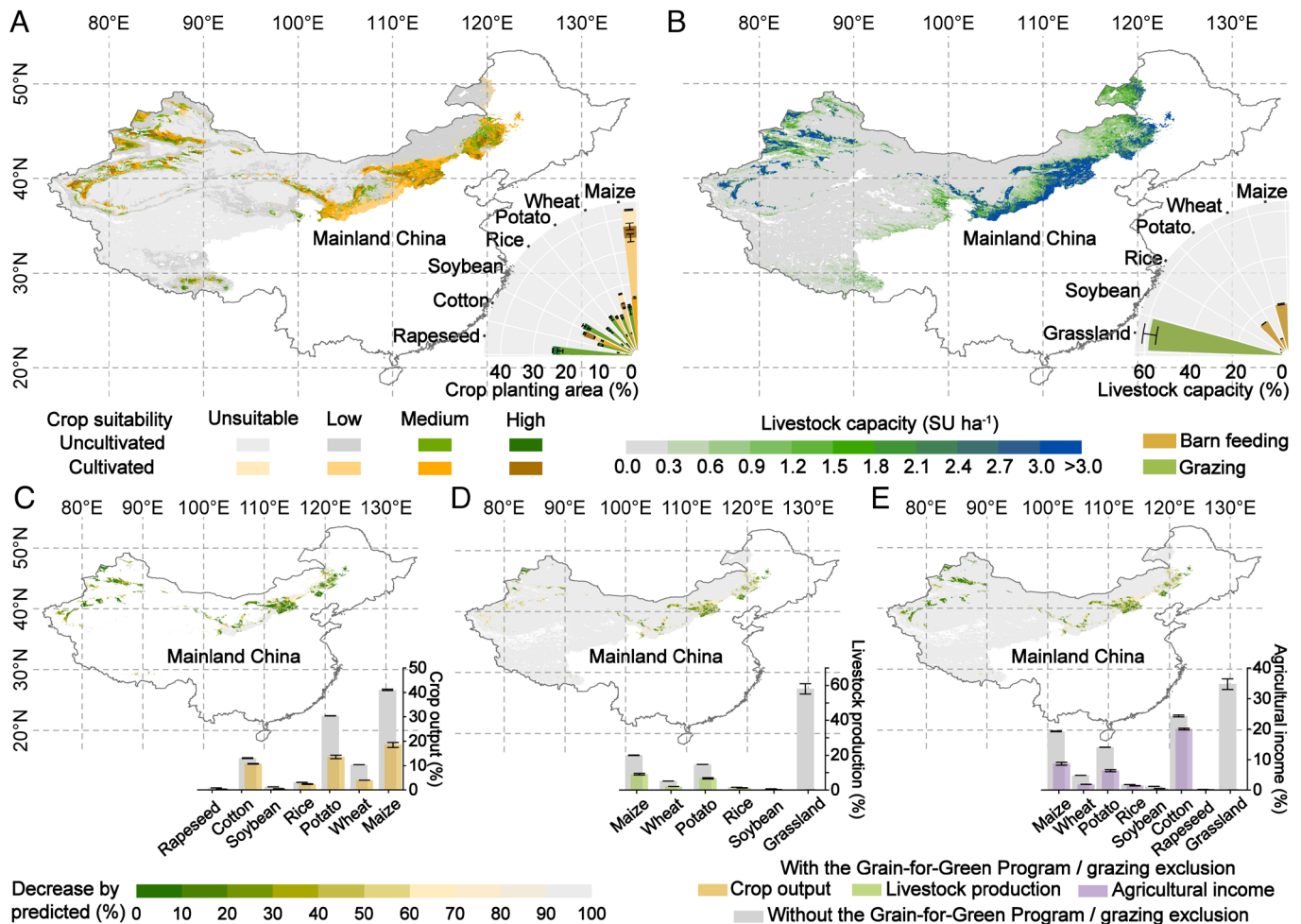
Fig. 2. Crop suitability, livestock capacity, and potential impacts of current desertification reversal strategies on agricultural production and income in China's desertification-prone regions for 2023–2050. Panels (*A*) and (*B*) show the distributions of crop suitability and livestock capacity, respectively, for this period, with legends consistent with Fig. 1 *A*, *B*, and *E*. Panels (*C–E*) illustrate the potential effects of maintaining current desertification reversal strategies on agricultural production and income from 2023 to 2050. The spatial maps display the projected percentage decreases in crop output, livestock production, and income after retiring unsuitable/low-suitability cropland and grazing exclusion on natural grasslands following implementation of current strategies. These are compared with the baseline scenario (no strategies). The bar charts summarize regional statistics for crop output, livestock production, and agricultural income, with cartographic elements consistent with Fig. 1 *F* and *G*. Both spatial maps and bar charts reflect simulated averages under the L1, M2, and H3 climate scenarios, with whiskers on the bar charts indicating the assessment ranges across scenarios. Independent crop suitability assessments for this period are shown in *SI Appendix*, Fig. S8.

0.9%, respectively. In contrast, strategies involving pasture cultivation and crop switching (S2–S4) are projected to increase vegetation cover by 0.2 (S2) to 0.6% (S4); increase livestock production by 5.1 (S2) to 35.2% (S4); and reduce ecological water deficits by 0.1 (S3) to 3.7% (S4). While these strategies may introduce trade-offs between crop outputs and agricultural incomes due to resource constraints, allocating land areas according to crop suitability can largely mitigate conflicts between economic development and desertification combating. Our findings also support this hypothesis, indicating that converting unsuitable cropland to natural grassland, transforming low-suitability cropland into cultivated pasture, and switching crops on medium- to high-suitability cropland (S3) synergistically increase crop output by up to 4.3% and agricultural income by over 20.5%.

We further assessed two additional radical agricultural development strategies aimed at addressing extreme food crises (S5 and S6). Our results indicated that fully utilizing high-suitability cropland while converting other cropland to cultivated pasture (S5) could increase livestock production by 35.3 to 40.1%, raise agricultural income by 0.0 to 5.3%, and enhance vegetation cover by 1.9 to 2.2%. However, this strategy also increases ecological

water deficits by 23.7 to 29.6%, while newly reclaimed land would fail to offset widespread crop abandonment, causing a 51.7 to 57.2% decline in crop output. Conversely, completely banning grazing in natural grasslands (S6) could dramatically increase vegetation cover by 55.7 to 60.4%, meanwhile at the cost of reducing livestock production by 15.3 to 18.4% and lowering agricultural income by 28.2 to 31.7%. The reimagined strategies to combat desertification projected divergent outcomes under future climate scenarios, enabling the cautious decision-making of desertification combating practices toward sustainability from multiple dimensions.

Discussion: Toward Sustainability in Combating Desertification.
Desertification remains a major obstacle to sustainable development, exacerbating poverty, food insecurity, and water scarcity in arid and semiarid regions (3, 13). Between 2000 and 2020, China invested ~470 billion RMB (~67 billion USD), equivalent to 3.19% of local fiscal revenues, in the Grain-for-Green Program and grazing exclusion (*SI Appendix*, Figs. S2 and S3). Yet despite generous subsidies—1,500 yuan ha^{-1} y^{-1} for cropland retirement and 37.5 to 112.5 yuan ha^{-1} y^{-1} for grazing exclusion—farmers and herders

Table 1. Strategies reimagined for combating desertification under future climate and sustainable development scenarios

Strategy	Description
S0	Maintain current agricultural practices and desertification combating strategies.
S1	Convert unsuitable or low suitability cropland into natural grassland and determine the grazing intensity in accordance with the carrying capacity in natural grasslands.
S2	Convert unsuitable cultivated cropland into natural grassland, convert low suitability cultivated cropland into cultivated pasture, and determine the grazing intensity in accordance with the livestock capacity in natural grasslands.
S3	Convert unsuitable cultivated cropland into natural grasslands, convert low-suitability cultivated cropland into cultivated pasture, switch crops in medium- to high-suitability cultivated cropland, and determine the grazing intensity in accordance with the livestock capacity in natural grasslands.
S4	Convert unsuitable cultivated cropland into natural grassland, convert low- to medium-suitability cultivated cropland into cultivated pasture, switch crops in high-suitability cultivated cropland, and determine the grazing intensity in accordance with the livestock capacity in natural grasslands.
S5	In addition to S4, fully exploit all areas suitable for crop planting and determine the grazing intensity in accordance with the livestock capacity in natural grasslands.
S6	In addition to S5, enforce the complete exclusion of grazing in natural grasslands.

Note: Current distributions of agricultural practices and their changes under different optimization strategies in China's desertification-prone regions are shown in *SI Appendix*, Fig. S9.

incurred much higher income losses (21,129.5 and 139.8 yuan ha^{-1} y^{-1}, respectively (Fig. 1*G*; 24). Given fiscal constraints, such subsidies were sustainable for only 5 to 10 y (24), rendering these strategies economically unsound and unviable for replication in low-income regions such as Sub-Saharan Africa or Central Asia. Besides fiscal limitations, ecological constraints also undermine the long-term effectiveness of large-scale greening initiatives, including the persistence of stable desert states that hinder forest recovery in some drylands (25, 26) and groundwater depletion caused by water-intensive species like eucalyptus (27, 28).

To address these limitations, we developed a scalable decision-making framework for combating desertification that integrates multiple statistical learning algorithms with high-resolution empirical evidence data and extensive environmental datasets (Fig. 4). Specifically, this framework incorporates 95 biophysical variables covering topography, soils, climate, and water availability. After rigorous sample screening and principal component analysis, these variables were coupled with niche and yield models to generate ~30 m resolution probabilistic maps of yield potential for major crops, natural grasslands, and cultivated pastures, achieving interpretability exceeding 95% (*Materials and Methods* and *SI Appendix, Supporting Text*). This methodological advance provides a robust foundation for quantifying the cobenefits of optimized resource allocation across combating desertification, socioeconomic development, and resource-use efficiency. More significantly, by simulating the outcomes of multiple optimized strategies, the framework operationalizes the principles of the SDGs and identifies locally tailored implementation pathways.

Application of this framework in China shows that advanced agricultural practices—especially crop switching and pasture cultivation on marginal croplands—can simultaneously mitigate ecological degradation, enhance rural livelihoods, and alleviate fiscal burdens. Warming-induced snowmelt is projected to increase water availability in certain ecologically fragile regions (*SI Appendix*, Fig. S7), creating opportunities for more strategic land-use adjustment (29, 30). Under such conditions, optimal redistribution of crops and pastures could offset yield losses from cropland retirement while reducing public expenditures on combating desertification by ~22 billion yuan (~3 billion USD) annually (*SI Appendix*, Figs. S2 and S3). These strategies, aligned with China's dietary guideline of 21 kg of meat cap^{-1} y^{-1} (31), the United Nations extreme poverty line of 1.90 USD (~13.57 yuan) cap^{-1} d^{-1}, and the World Health Organization minimum water threshold of 50 L of water cap^{-1} d^{-1} (7), could between 2023 and 2050 sustain adequate protein intake for 71.78 million people, lift 7.87 million individuals out of extreme poverty, and mitigate water scarcity for 136.10 million people (Fig. 3). Collectively, these benefits advance 0.7% of SDG 1 (out of 1.1 billion in extreme poverty), 9.8% of SDG 2 (out of 733 million facing hunger), and 3.8% of SDG 6 (out of 3.6 billion lacking safe water) (7). Beyond these direct gains, synergies in crop and livestock production and vegetation restoration (Fig. 3) create cascading benefits across international cooperation (32, 33), supporting SDGs 10 (reduced inequalities), 12 (responsible consumption), 13 (climate action), 15 (life on land), and 17 (partnerships) (*SI Appendix*, Table S1). Given that similar agricultural practices are already widespread worldwide (20–23), the benefits demonstrated in China are both scalable and globally relevant.

Nonetheless, cautious management of trade-offs among SDGs, particularly those concerning food security, water conservation, and vegetation recovery, is essential. Our findings indicate that expanding crop and livestock productivity to secure food supplies risks worsening water scarcity, while prioritizing water conservation may reduce agricultural profitability, and maximizing vegetation restoration can displace land-dependent households (Fig. 3). Moreover, achieving optimal outcomes for water conservation (S4 in Table 1), agricultural profit (S3), or vegetation recovery (S6) requires reallocating 26.3 to 31.2 million hectares of land (Fig. 3 and *SI Appendix*, Fig. S9), necessitating substantial labor and financial investments. These tensions underscore both the complexity of combating desertification and the broader challenge of reconciling competing SDGs under finite resource constraints (3, 34). Addressing these challenges requires coordinated efforts across communities, institutions, governments, and international partners (35), supported by high-resolution environmental data, reliable climate projections, and region-specific socioeconomic assessments. By critically engaging with global frameworks while grounding solutions in local realities, our work highlights a promising pathway for combating desertification that balances global aspirations with regional feasibility, thereby advancing both the scientific understanding and the practical implementation of sustainable development.

Materials and Methods

Data sources and processing methods are detailed in *SI Appendix, Supporting Text*. Below is an overview of the main models and methods.

Crop Suitability Assessment. We developed crop suitability assessment models for maize, wheat, cotton, potatoes, rice, soybeans, and rapeseed, which represent ~68.8% of the total sown area in China's desertification-prone regions (*SI Appendix*, Table S2), using the maximum entropy algorithm (36, 37). National
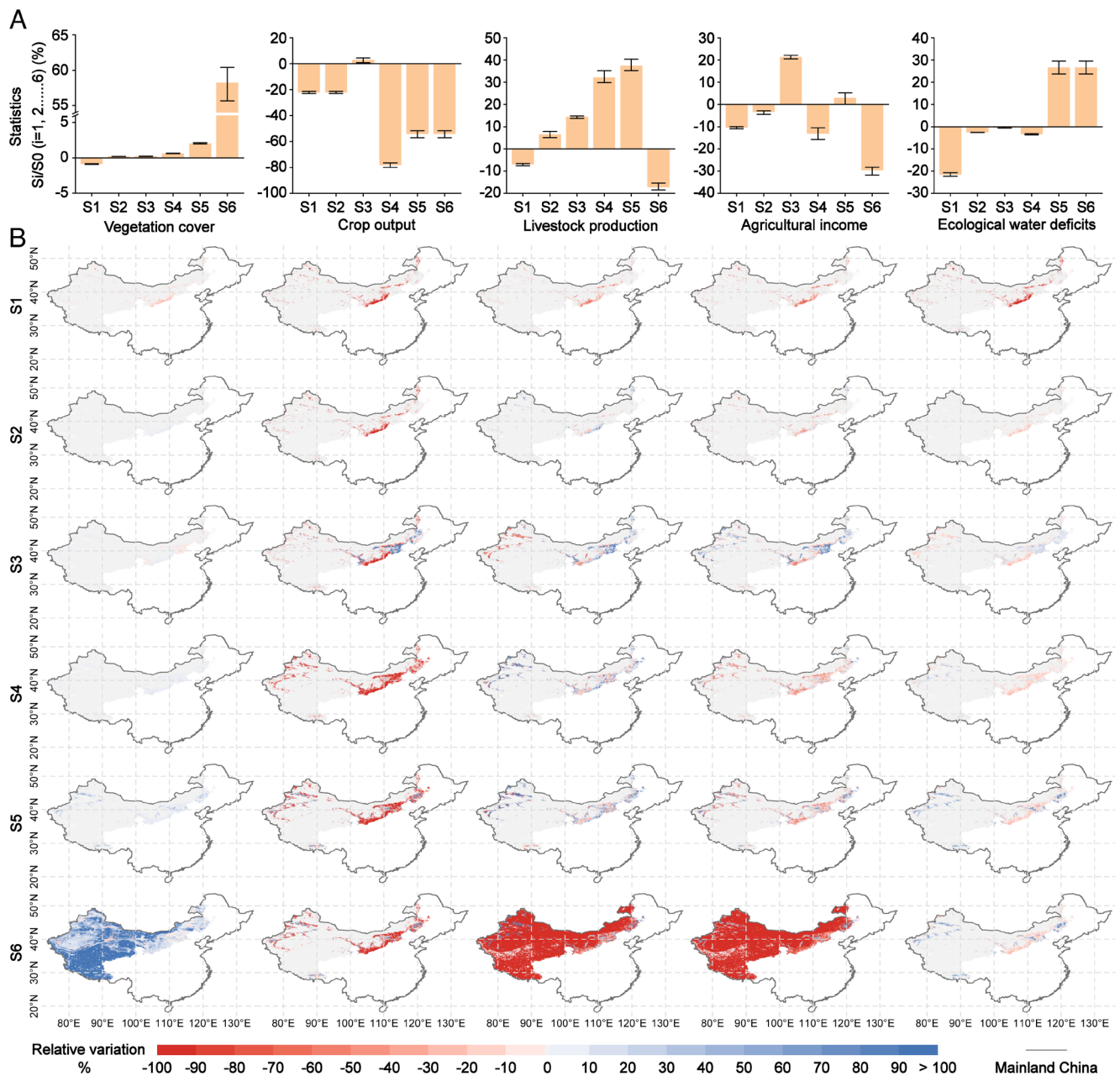
Fig. 3. Changes in vegetation cover, crop output, livestock production, agricultural income, and ecological water deficit in China's desertification-prone regions (2023–2050) under optimized strategies, compared with current desertification combating and agricultural practices. Panel (*A*) displays regional statistics reflecting relative changes in each evaluation index under optimized strategies. Panel (*B*) shows the spatial distributions of these relative changes for strategies S1–S6 (arranged from *Top* to *Bottom*). Vegetation cover for each geographic unit is calculated as the area-weighted average of crop and grassland components, while the other indicators are based on the sums of these components. Both spatial maps and bar charts represent simulated averages under L1, M2, and H3 climate scenarios, with whiskers on the bar charts indicating the assessment ranges across scenarios. Details of the optimized strategies are provided in Table 1. Changes in agricultural production area under each strategy are shown in *SI Appendix*, Fig. S9, and comprehensive statistics for all indicators (S0–S6) are presented in *SI Appendix*, Figs. S10–S14.

average yields for these crops were calculated from the SPAM 2020 v1.0 dataset provided by the International Food Policy Research Institute (https://mapspam.info/data/) (*SI Appendix*, Table S3). We identified ~10-km resolution grids where observed yields exceeded national averages and extracted farmland patch centroids within these grids using ArcGIS 10.6 to serve as ecological niche samples.

Dynamic predictors included seven monthly climatic variables (cumulative precipitation, mean/maximum/minimum daily temperature, downward shortwave solar radiation, mean wind speed, and terrestrial water storage) and four annual climatic variables (number of days > 0 °C, effective accumulated temperature days > 0 °C, and mean atmospheric CO_2 concentration). Static predictors encompassed slope, elevation, soil type and texture (sandy/silty/clay), and distance to rivers and roads (*SI Appendix*, Fig. S15 and Table S4). To reduce multicollinearity among 95 environmental factors, we performed

principal component analysis and retained components that explained 99% of the cumulative variance (*SI Appendix*, Table S5).

Suitability models were constructed using the maxent function in the *dismo* package (R 4.0.4), producing suitability probability surfaces (*P*) classified via the natural breaks method into highly suitable ($P \geq 0.7$), moderately suitable ($0.7 > P \geq 0.5$), low suitability ($0.5 > P \geq 0.1$), and unsuitable ($P < 0.1$) areas (38). Low-suitability or unsuitable croplands were prioritized for combating desertification, while moderate and highly suitable lands were maintained for agricultural production.

Crop Yield Estimation. We developed random forest models to predict yields for the same seven crops using SPAM 2020 v1.0 dataset (10-km resolution, 2019–2021 averages). For each crop, data on annual average harvested area,
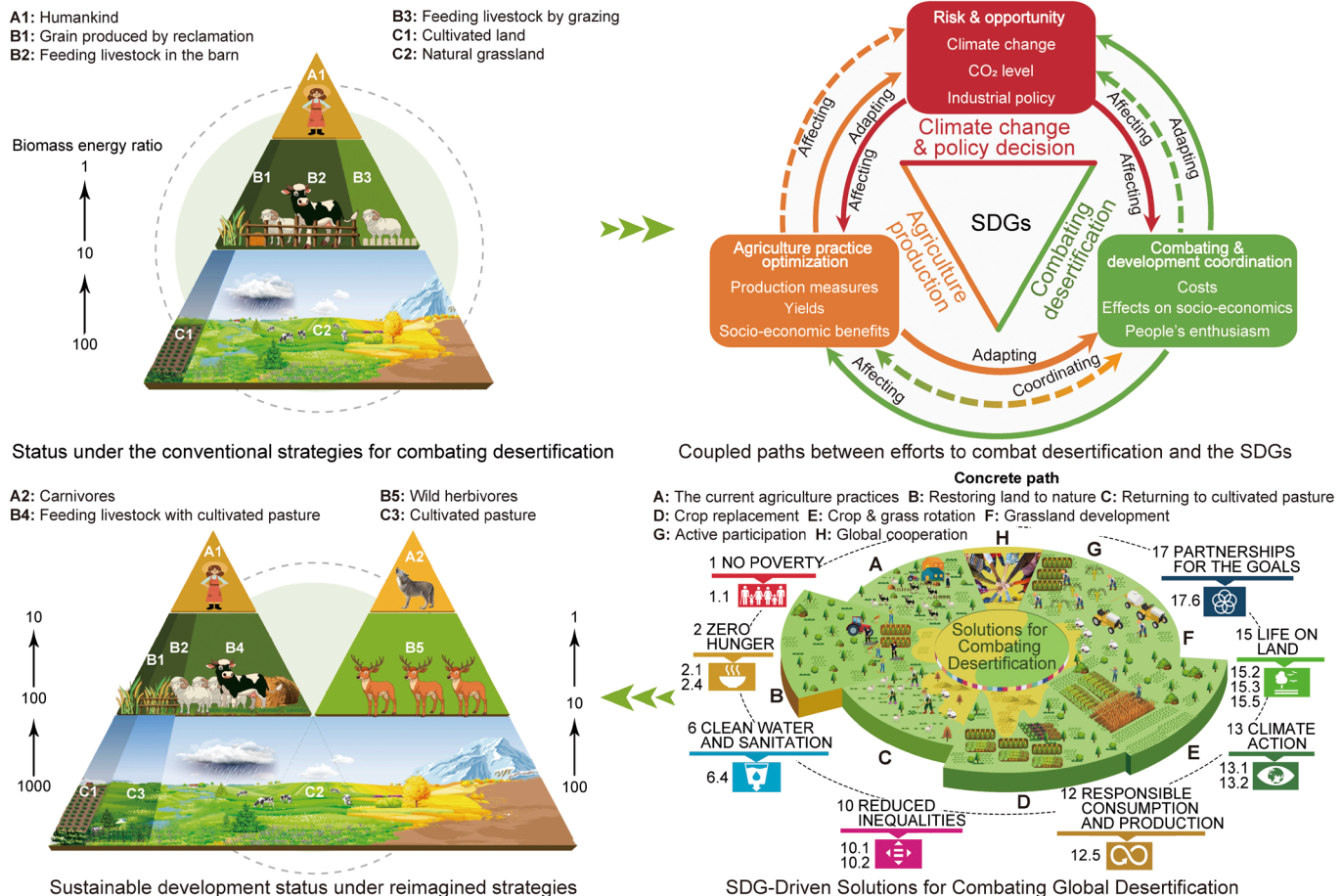
Fig. 4. Sustainable pathways for reimagined desertification reversal strategies. The *Upper-Left* panel illustrates the conventional strategies, which primarily emphasize superficial vegetation greening while often overlooking the interests of key stakeholders. In contrast, the *Bottom-Left* panel depicts the potential status of sustainable development after optimization. This reimaging of efforts to combat desertification can substantially increase land-use efficiency and carrying capacity, thereby fostering a win–win scenario for future socioeconomic and ecological development. The *Right* panels outline specific pathways proposed to align China's initiatives to combat desertification with the SDGs. By optimizing agricultural practices in anticipation of climate change, both the effectiveness of desertification combating and public engagement can be synergistically enhanced. These improvements directly support SDGs 1, 2, and 6, and are expected to increase vegetation cover in desertification-prone regions by 2050 (Table 1 and Fig. 3), while also contributing SDGs 10, 12, 13, 15, and 17 through international cooperation.

per-unit-area yield, and geographic coordinates were extracted under both rainfed and irrigated conditions. Harvested area data were resampled to 1-km grids by allocating crop areas to the 10-km base grid in ArcGIS 10.6, followed by natural neighbor interpolation. Planting area proportions within each 1-km cell were then calculated to generate high-resolution crop distribution maps (*SI Appendix*, Fig. S9 *A–G*). Invalid points without sown area were excluded, and sampling was performed on all remaining valid points (*SI Appendix*, Table S3). Sample coordinates were adjusted to match the centroids of 30-m farmland polygons.

Random forest models were trained on these high-resolution datasets. Multiple bootstrap subsets were generated, each used to train an independent classification and regression tree (CART). Optimal splits were determined by information gain or the Gini index, and predictions from 50 CARTs were averaged to produce the final yield estimates, thereby balancing computational efficiency, accuracy, and control overfitting (39). In each iteration, 70% of samples were used for training and 30% for testing. Driving factor selection and principal component inputs followed the same procedure as in the suitability model (*SI Appendix*, Tables S4 and S5). All modeling and simulations were implemented in R 4.0.4 using the *randomForest* package.

Livestock Capacity Estimation. We initially reconstructed aboveground biomass (*AGB*) per unit area using a 250-m resolution normalized difference vegetation index (*NDVI*) dataset (1982–2022), based on the empirical model of Piao et al. (40) as follows (Eq. **1**):

$$AGB = 291.64 \times NDVI^{1.5842} \quad (R^2 = 0.72, \ P < 0.001),　[1]$$

where *AGB* is expressed in g C m^{-2} and *NDVI* is derived from the red and infrared bands.

Using available AGB data as training samples, we extended estimates to 1961–2050 via stepwise multiple linear regression (Eq. **2**):

$$AGB = b + \sum_{i \in env} a_i x_i + \varepsilon,　[2]$$

where *env* denotes the set of potential driving factors consistent with the crop suitability assessment model parameters, *i* indicates a specific factor, *a* and *b* are regression parameters, *x* is the driving factor, and *ε* is the residual. Feature selection at the grid-cell scale was performed using the Akaike Information Criterion (AIC), where lower values indicate better model simplicity/accuracy trade-offs.

We then applied two conversion factors, *TreeCoverMultiplier* and *SlopesMultiplier*, to constrain livestock-accessible AGB (41). The adjusted biomass (*AGB'*, g C m^{-2}) was defined as follows (Eqs. **3–5**):

$$AGB' = AGB \times TreeCoverMultiplier \times SlopesMultiplier,　[3]$$

$$TreeCoverMultiplier = \frac{1}{e^{4.45521 \times TreeCover}},　[4]$$

$$SlopeMultiplier = \begin{cases} 1.0 & 0\% \leq Slope < 10\% \\ 0.7 & 10\% \leq Slope < 30\% \\ 0.4 & 30\% \leq Slope < 60\% \\ 0.0 & 60\% \leq Slope < 100\% \end{cases},　[5]$$

where *TreeCover* denotes multiyear average canopy coverage (%).

Based on Holecheck et al. (42), herbivores consume 1.8 to 4.0% of body weight in dry matter daily. For a 50-kg standard SU, the daily intake is calculated as 0.5 × (50 kg × 1.8% + 50 kg × 4.0%). Grassland utilization rates (*A*, *SI Appendix*, Table S6) and regrowth rates (*G*, *SI Appendix*, Table S7) were set according to China's *grassland-livestock balance guidelines* (LY/T3320-2022) and grassland growth types datasets, including the 1:1,000,000 Vegetation Atlas of China (https://www.plantplus.cn/doi/10.12282/plantdata.0155) and the China Vegetation Zoning Dataset (https://www.resdc.cn/data.aspx?DATAID=133). Natural grasslands carrying capacity was calculated as (Eq. **6**):

$$CC = \frac{AGB'}{1.45 \times 1000 \times 365 \times 0.47} \times 10^4 \times A \times (1+G), \quad [6]$$

where *CC* is livestock carrying capacity in natural grasslands (SU ha^{-1}), and 0.47 is the conversion factor from dry matter to carbon mass.

For cultivated pasture, with an average harvest height of 80.37 ± 31.67 cm (43–45) and five annual cuts leaving 5-cm stubble, carrying capacity (*CC*$_{ag}$, SU km^2) was estimated as (Eq. **7**):

$$CC_{ag} = \frac{AGB'}{1.45 \times 1000 \times 365 \times 0.47} \times 10^4 \times A \times (1+G) \times 5 \\ \times \left(\frac{80.37-5}{80.37}\right), \quad [7]$$

where (80.37−5)/80.37 represents the harvestable forage proportion per cut, and the scaling factor adjusts for area.

Barn or pen feeding is a common livestock production method in desertification-prone regions. However, cross-regional feed transactions introduce significant uncertainties into agricultural cost–benefit assessments (46, 47), which fall outside the scope of this study. Consequently, we assumed that all barn feeding feedstock originates from local agricultural production. We further assumed that producers utilize local grassland resources sustainably and that barn feeding operations can accommodate stocking rates exceeding grazing capacity, consistent with China's *Technical Specification for Grass–Livestock Balance Assessment* (LY/T3320-2022). Since county-level livestock inventory data were unavailable before 1991, we compiled average year-end standard SU inventories for 1991–2022 using Chinese statistical yearbooks, prioritizing completeness and reliability. The annual barn fed stocking rate was then calculated by subtracting the reasonable grazing capacity of natural grasslands during this period. Feed crop consumption was subsequently estimated (*Yields*$_{dflot feeding}$, Eq. **8**). Our analysis shows that 30.82% of regional grain crop output supports barn feeding operations (*SI Appendix*, Table S8).

$$Yields_{drylot\ feeding} = CC_{drylot\ feeding} \times 1.45 \times 1000 \times 365 \times 0.47 \\ \times \frac{9.02}{16.07} \times 10^4, \quad [8]$$

where *CC*$_{drylot feeding}$ denotes the barn feeding stocking rate per unit area (SU ha^{-1}), and 9.02 and 16.07 represent the average digestible energy values (MJ kg^{-1}) for forage and grain, respectively.

Production and Income Evaluation. Based on potential per-unit-area yields of seven major grain crops (1961–2050), carrying capacities of natural grasslands and cultivated pasture, and per-unit-area producer incomes, we evaluated agricultural production and income under various scenarios (Eqs. **9** and **10**, respectively):

$$P_i = \sum_z HA_{i,z} \times PU_{i,z}, \quad [9]$$

$$I_i = \sum_z HA_{i,z} \times PU_{i,z} \times IU_{i,z}, \quad [10]$$

where the subscript *i* denotes a specific grid cell, *z* denotes a particular crop or livestock product, *HA* is the harvested area of the product, *P* is agricultural production, *I* is income, *PU* is the per-unit-area yield, and *IU* is the net profit per unit area (*SI Appendix*, Table S9).

Ecological Water Deficit Assessment. We applied a process-based crop water use model to evaluate the impacts of cultivation on local water resources and stress. Daily potential evapotranspiration (*ET*$_0$, mm) at 1,000-m resolution was first calculated using the Penman-Monteith equation. Crop coefficients (*K*$_z$) were

then calibrated, and total crop water requirements (*ET*$_z$, mm) were estimated following Allen et al. (48) and Xie et al. (49), accounting for climatic conditions in China's desertification-prone regions (Eqs. **11** and **12**).

$$K_Z = K_{Z(tab)} + \left[0.04(u_2-2) - 0.004(RH_{min}-45)\right]\left(\frac{h}{3}\right)^{0.3}, \quad [11]$$

$$ET_Z = K_Z \times ET_0, \quad [12]$$

where *K*$_{Z(tab)}$ denotes the tabulated crop coefficient by growth stage (*SI Appendix*, Table S10), *RH*$_{min}$ is the mean daily minimum relative humidity for each growth stage (%), and *h* is the average crop height at each growth stage (m) (*SI Appendix*, Table S10).

The ecological water deficit, after excluding effective rainfall, was defined as (Eqs. **13** and **14**):

$$BW_Z = \sum MAX\ (0, ET_{t,Z} - PRE_{eff,t}), \quad [13]$$

$$PRE_{eff} = \begin{cases} PRE \times (4.17 - 0.2 \times PRE)/4.17 & PRE < 8.3\ mm\ d^{-1} \\ 4.17 + 0.1 \times PRE & PRE \geq 8.3\ mm\ d^{-1} \end{cases}, \quad [14]$$

where *BW*$_Z$ (mm) is locally sourced water consumed, the subscript *t* denotes a specific crop or pasture growth stage, and *PRE*$_{eff,t}$ (mm) is cumulative effective rainfall (mm), modeled as a quadratic function of actual rainfall (*PRE*, mm). The crop growth cycle is described in *SI Appendix*, Table S11. Based on primary cropping patterns and desertification assessment criteria (50, 51), supplemental water was allowed only during early, rapid, and mid-growth stages.

Vegetation Cover Changes Assessment. We calculated fractional vegetation cover (*FVC*, %) at the grid scale using linear spectral unmixing (Eq. **15**):

$$FVC_i = \frac{NDVI_i - NDVI_{soil}}{NDVI_{veg} - NDVI_{soil}}, \quad [15]$$

where *FVC*$_i$ and *NDVI*$_i$ denote the FVC and NDVI values, respectively, for grid *i*, and *NDVI*$_{soil}$ and *NDVI*$_{veg}$ represent the NDVI values for bare soil and dense forests, respectively. Annual maximum NDVI values were extracted from long-term data (1980–2020) for areas with stable bare soil and dense forest cover. The 5th and 95th percentile NDVI values, 0.034 and 0.910, were identified as reference values for *NDVI*$_{soil}$ and *NDVI*$_{veg}$, respectively.

To evaluate vegetation cover under various scenarios, we developed nine random forest models covering seven major crops, natural grassland, and cultivated pasture. FVC sampling points for crops were aligned with those used in yield modeling. For natural grasslands, 10,000 random sampling points were selected in pastoral areas. For cultivated pasture, an additional 10,000 points were randomly selected within 5 km of the cultivated cropland boundaries, focusing on the top 20% of FVC values observed in pastoral areas. Modeling and validation procedures followed the same framework as in crop yield estimation.

Finally, we simulated FVC changes during grazing (1982–2002) and grazing-exclusion (2003–2022) periods following Wang et al. (4). Using 2003 as the baseline, with identical sampling and parameter settings (*SI Appendix*, Table S4), we quantified vegetation cover differences with and without grazing exclusion.

Robustness Analysis. The quality of the crop suitability model was assessed using the area under the receiver operating characteristic curve (AUC) (52). AUC values range from 0.5 to 1, with higher values indicating better performance. After 10 repetitions, all crops achieved AUC values above 0.95, demonstrating excellent accuracy (*SI Appendix*, Fig. S16). For crop yield estimation, performance was evaluated using the Pearson correlation coefficient (*r*), mean absolute error (*MAE*), coefficient of determination (*R*^{2}), and Kling-Gupta efficiency coefficient (*KGE*). Results showed *r*, *R*^{2}, and *KGE* values ranging from 0.96 to 0.99, 0.91 to 0.98, and 0.87 to 0.96, respectively. MAE values were below 8% for all crops except rice (12.03%), confirming excellent performance (*SI Appendix*, Table S12). Model outputs were further validated at county/district and field scales during the modeling period (2019–2021) (*SI Appendix*, Fig. S17), with regional yield deviations from Chinese official statistics of −0.09 to −2.06%. Yield estimation uncertainty primarily reflects variability in climatic models. The reliability of AGB fitting equations was tested using the spatial distributions of *r*, *MAE*, and *R*^{2} (*SI Appendix*, Fig. S18). Random

forest-based FVC model evaluations (*SI Appendix*, Table S13) also confirmed consistently high reliability. Ecological water deficit estimates, derived from physically based models with locally calibrated parameters, showed stable uncertainties across climate and strategy scenarios. As a result, error bands in crop water consumption requirements tend to offset when comparing optimized outcomes.

Data, Materials, and Software Availability. Historical climate data were obtained from the ERA5 atmospheric reanalysis produced by the European Centre for Medium-Range Weather Forecasts and accessed via the Copernicus Climate Data Store (https://cds.climate.copernicus.eu/) (53). Future climate data were obtained from the Coupled Model Intercomparison Project Phase 6 (CMIP6) archive (https://aims2.llnl.gov/search/cmip6/) (54). Land-use data were obtained from the Land Use/Land Cover Remote Sensing Monitoring Dataset of China (CNLUCC; https://www.resdc.cn/) (55). NDVI data were obtained from the blended vegetation health product provided by the NOAA Center for Satellite Applications and Research (https://www.star.nesdis.noaa.gov/) (56) and from the MODIS MOD13Q1 product distributed by the NASA Level-1 and Atmosphere Archive & Distribution System Distributed Active Archive Center (https://ladsweb.modaps.eosdis.nasa.gov/) (57). Crop harvested area and yield data were obtained from the SPAM 2020 v1.0 dataset provided by the International Food Policy Research Institute (https://mapspam.info/data/) (58). Socioeconomic data were compiled from official statistical databases of Chinese administrative regions, government reports, and the literature, as included in the article and/or *SI Appendix*.

Author affiliations: ᵃInstitute of Geographic Sciences and Natural Resources Research, Chinese Academy of Sciences, Beijing 100101, China; ᵇCollege of Resources and Environment, University of Chinese Academy of Sciences, Beijing 100049, China; ᶜState Key Laboratory of Tibetan Plateau Earth System, Environment and Resources, Institute of Tibetan Plateau Research, Chinese Academy of Sciences, Beijing 100101, China; ᵈGlobal Ecology Unit, Centre for Ecological Research and Forestry Applications-National Research Council-Universitat Autonoma de Barcelona, Bellaterra, Catalonia 08193, Spain; ᵉCommonwealth Scientific and Industrial Research Organisation, Waite Campus, Adelaide, SA 5064, Australia; ᶠCentre for Integrative Ecology, Deakin University, Geelong, VIC 3217, Australia; ᵍState Key Laboratory of Earth Surface Processes and Resource Ecology, Faculty of Geographical Science, Beijing Normal University, Beijing 100875, China; ʰInstitute of Land Surface System and Sustainable Development, Faculty of Geographical Science, Beijing Normal University, Beijing 100875, China; ᶦDepartment of Environment and Geography, University of York, York YO10 5DD, United Kingdom; ʲYork Environmental Sustainability Institute, University of York, York YO10 5DD, United Kingdom; ᵏState Key Laboratory of Herbage Improvement and Grassland Agro-ecosystems, College of Ecology, Lanzhou University, Lanzhou 730000, China; ˡCollege of Atmospheric Sciences, Lanzhou University, Lanzhou 730000, China; ᵐKey Laboratory of Cenozoic Geology and Environment, Institute of Geology and Geophysics, Chinese Academy of Sciences, Beijing 100029, China; ⁿSchool of Geography and Ocean Science, Nanjing University, Nanjing 210023, China; ᵒState Key Laboratory of Severe Weather, Institute of Atmospheric Composition, Chinese Academy of Meteorological Sciences, Beijing 100081, China; ᵖCollege of Urban and Environmental Sciences, Peking University, Beijing 100871, China; ᑫEducation and Research Department, Beijing Changjier Education Foundation, Beijing 100028, China; ʳSchool of Geography and the Environment, University of Oxford, Oxford OX1 3QY, United Kingdom; ˢSchool of Geography and Tourism, Shaanxi Normal University, Xi'an 710119, China; ᵗSchool of Management, Minzu University of China, Beijing 100081, China; ᵘShaanxi Key Laboratory of Earth Surface System and Environmental Carrying Capacity, College of Urban and Environmental Science, Northwest University, Xi'an 710127, China; ᵛXinjiang Institute of Ecology and Geography, Chinese Academy of Sciences, Urumqi 830011, China; and ʷKey Laboratory of Desert and Desertification, Northwest Institute of Eco-Environment and Resources, Chinese Academy of Sciences, Lanzhou 730000, China

1. UNCCD, *United Nations Convention to Combat Desertification in Countries Experiencing Serious Drought and/or Desertification, particularly in Africa* (UNCCD, France, Paris, 1994). https://www.unccd.int/sites/default/files/2022-02/UNCCD_Convention_ENG_0_0.pdf.
2. C. Li *et al.*, Drivers and impacts of changes in China's drylands. *Nat. Rev. Earth Environ.* **2**, 858–873 (2021).
3. UNCCD, *Global Land Outlook* (UNCCD, ed. 2, Bonn, 2022). https://www.unccd.int/sites/default/files/2022-04/UNCCD_GLO2_low-res_2.pdf.
4. X. Wang *et al.*, Unintended consequences of combating desertification in China. *Nat. Commun.* **14**, 1139 (2023).
5. P. Meyfroidt *et al.*, Ten facts about land systems for sustainability. *Proc. Natl. Acad. Sci. U.S.A.* **119**, e2109217118 (2022).
6. C. Parr, M. Beest, N. Stevens, Conflation of reforestation with restoration is widespread. *Science* **383**, 698–701 (2024).
7. United Nations General Assembly, *Transforming Our World: The 2030 Agenda for Sustainable Development* (United Nations, New York, 2015). https://www.refworld.org/legal/resolution/unga/2015/en/111816.
8. X. Wang *et al.*, Desert ecosystems in China: Past, present, and future. *Earth-Sci. Rev.* **234**, 104206 (2022).
9. B. Bryan *et al.*, China's response to a national land-system sustainability emergency. *Nature* **559**, 193–204 (2018).
10. C. Li *et al.*, Climate-driven ecological thresholds in China's drylands modulated by grazing. *Nat. Sustain.* **6**, 1363–1372 (2023).
11. F. Lu *et al.*, Effects of national ecological restoration projects on carbon sequestration in China from 2001 to 2010. *Proc. Natl. Acad. Sci. U.S.A.* **115**, 4039–4044 (2018).
12. L. Cheng *et al.*, Estimation of the costs of desertification in China: A critical review. *Land Degrad. Dev.* **29**, 975–983 (2018).
13. J. Reynolds *et al.*, Global desertification: Building a science for dryland development. *Science* **316**, 847–851 (2007).
14. S. Cao *et al.*, Development and testing of a sustainable environmental restoration policy on eradicating the poverty trap in China's Changting County. *Proc. Natl. Acad. Sci. U.S.A.* **106**, 10712–10716 (2009).
15. World Trade Organization, WTO Global trade data portal (2025). https://globaltradedata.wto.org/official-data.
16. X. Feng *et al.*, Revegetation in China's Loess Plateau is approaching sustainable water resource limits. *Nat. Clim. Change* **6**, 1019–1022 (2016).
17. S. Rohatyn, D. Yakir, E. Rotenberg, Y. Carmel, Limited climate change mitigation potential through forestation of the vast dryland regions. *Science* **377**, 1436–1439 (2022).
18. Y. Chen *et al.*, Balancing green and grain trade. *Nat. Geosci.* **8**, 739–741 (2015).
19. F. Maestre *et al.*, Grazing and ecosystem service delivery in global drylands. *Science* **378**, 915–921 (2022).
20. M. Eisler *et al.*, Agriculture: Steps to sustainable livestock. *Nature* **507**, 32–34 (2014).
21. International Center for Agricultural Research in the Dry Areas (ICARDA), Integrated Desert Farming Innovation Program (IDFIP) (2023). https://icarda.org/research/integrated-desert-farming-innovation-program. Accessed 15 December 2023.
22. K. Davis *et al.*, Increased food production and reduced water use through optimized crop distribution. *Nat. Geosci.* **10**, 919–924 (2017).
23. I. Elouafi, Drylands under pressure: Science and solutions for global stability. *Science* **387**, eadv6563 (2025).
24. National Forestry and Grassland Administration, *China Forestry and Grassland Statistical Yearbook (1998–2018)* (China Forestry Publishing House, Beijing, 1998–2018).
25. P. D'Odorico, A. Bhattachan, K. Davis, S. Ravi, C. Runyan, Global desertification: Drivers and feedbacks. *Adv. Water Res.* **51**, 326–344 (2013).
26. C. Runyan, P. D'Odorico, D. Lawrence, Physical and biological feedbacks of deforestation. *Rev. Geophys.* **50**, RG4006 (2012).
27. P. D'Odorico, J. Dell'Angelo, M. Rulli, Appropriation pathways of water grabbing. *World Dev.* **181**, 106650 (2024).
28. L. Ricciardi, P. D'Odorico, N. Galli, D. Chiarelli, M. Rulli, Hydrological implications of large-scale afforestation in tropical biomes for climate change mitigation. *Phil. Trans. R. Soc. Lond. B Biol. Sci.* **377**, 20210391 (2022).
29. H. Pritchard, Asia's shrinking glaciers protect large populations from drought stress. *Nature* **569**, 649–654 (2019).
30. T. Smith, N. Boers, Global vegetation resilience linked to water availability and variability. *Nat. Commun.* **14**, 498 (2023).
31. Chinese Nutrition Society (CNS), *The Chinese Dietary Guidelines* (People's Medical Publishing House of China, 2016).
32. K. Schmidt, A. Ockenfels, Focusing climate negotiations on a uniform common commitment can promote cooperation. *Proc. Natl. Acad. Sci. U.S.A.* **118**, e2013070118 (2021).
33. C. Folberth *et al.*, The global cropland-sparing potential of high-yield farming. *Nat. Sustain.* **3**, 281–289 (2020).
34. F. Maestre *et al.*, Bending the curve of land degradation to achieve global environmental goals. *Nature* **644**, 347–355 (2025).
35. Y. You, N. Zhou, Y. Wang, Comparative study of desertification control policies and regulations in representative countries of the Belt and Road Initiative. *Glob. Ecol. Conserv.* **27**, e01577 (2021).
36. S. Phillips, R. Anderson, R. Schapire, Maximum entropy modeling of species geographic distributions. *Ecol. Modell.* **190**, 231–259 (2006).
37. E. Foerderer, D. Roedder, M. Langer, Global diversity patterns of larger benthic foraminifera under future climate change. *Glob. Change Biol.* **29**, 969–981 (2022).
38. J. Lin *et al.*, Predicting future urban waterlogging-prone areas by coupling the maximum entropy and FLUS model. *Sustain. Cities Soc.* **80**, 103812 (2022).
39. A. Liaw, M. Wiener, Classification and regression by randomForest. *R News* **2**, 18–22 (2002).
40. S. Piao, J. Fang, L. Zhou, K. Tan, S. Tao, Changes in biomass carbon stocks in China's grasslands between 1982 and 1999. *Glob. Biogeochem. Cycles* **21**, GB2002 (2007).
41. J. Piipponen *et al.*, Global trends in grassland carrying capacity and relative stocking density of livestock. *Glob. Change Biol.* **28**, 3902–3919 (2022).
42. J. Holechek, R. Pieper, C. Herbel, *Range Management: Principles and Practices* (Prentice Hall, ed. 6, 2010), https://aalto.finna.fi/Record/alli.899741.
43. B. Feng, Z. Liu, T. Baoyin, H. Tang, Effects of mowing frequency on community characteristics of dry mixed sowing artificial pasture. *Chin. J. Grassl.* **43**, 10–18 (2021).
44. Y. Zhao, *Changes of Agricultural Climate Resources in Hedong Region of Gansu and Its Impacts on Local Agriculture and Animal Husbandry in the Last 50 Years* (Northwest Normal University, 2013).
45. G. Qu, *The investigation on the introduction of herbage and forage crop in agricultural area of Tibetan* (Chinese Academy of Agricultural Sciences, 2012).

46. T. Kastner, K. Erb, H. Haberl, Rapid growth in agricultural trade: Effects on global area efficiency and the role of management. *Environ. Res. Lett.* **9**, 034015 (2014).

47. A. Ortiz, C. Outhwaite, C. Dalin, T. Newbold, A review of the interactions between biodiversity, agriculture, climate change, and international trade: Research and policy priorities. *One Earth* **4**, 88–103 (2021).

48. R. Allen, L. Pereira, D. Raes, M. Smith, Crop evapotranspiration-Guidelines for computing crop water requirements. *FAO irrig. drain. pap No. 56* **300**, D05109 (1998).

49. W. Xie *et al.*, Crop switching can enhance environmental sustainability and farmer incomes in China. *Nature* **616**, 300–305 (2023).

50. J. Heinke *et al.*, Water use in global livestock production-Opportunities and constraints for increasing water productivity. *Water Resour. Res.* **56**, e2019WR026995 (2020).

51. K. Descheemaeker, T. Amede, A. Haileslassie, Improving water productivity in mixed crop-livestock farming systems of sub-Saharan Africa. *Agric. Water Manage.* **97**, 579–586 (2010).

52. R. Halvorsen *et al.*, How important is the choice of model selection method and spatial autocorrelation of presence data. For distribution modelling by MaxEnt? *Ecol. Model.* **328**, 108–118 (2016).

53. European Centre for Medium-Range Weather Forecasts (ECMWF), ERA5 atmospheric reanalysis data. Copernicus Climate Data Store. https://cds.climate.copernicus.eu/. Accessed 16 October 2025.

54. World Climate Research Programme (WCRP), Coupled Model Intercomparison Project Phase 6 (CMIP6) model output. Earth System Grid Federation. https://aims2.llnl.gov/search/cmip6/. Accessed 16 October 2025.

55. X. Xu *et al.*, Data Registration and Publishing System of the Resource and Environmental Science Data Center of the Chinese Academy of Sciences. China's Multi-Period Land Use Land Cover Remote Sensing Monitoring Dataset. https://doi.org/10.12078/2018070201. Accessed 16 October 2025.

56. NOAA Center for Satellite Applications and Research, Blended Vegetation Health (BVH) NDVI product. NOAA STAR. https://www.star.nesdis.noaa.gov/smcd/emb/vci/VH/vh_ftp.php. Accessed 16 October 2025.

57. NASA Level-1 and Atmosphere Archive & Distribution System Distributed Active Archive Center (LAADS DAAC), MODIS MOD13Q1 vegetation indices product. NASA Earth Observing System Data and Information System. https://ladsweb.modaps.eosdis.nasa.gov/missions-and-measurements/products/MOD13Q1. Accessed 16 October 2025.

58. International Food Policy Research Institute (IFPRI), Spatial Production Allocation Model (SPAM) 2020 v1.0 global crop production data. MapSPAM database. https://mapspam.info/data/. Accessed 16 October 2025.